Design and Analysis of Cooling Systems for Combustion Chambers in Turbine Engines: A Comparison of Oil and Gas Cooling Fluids

Sourav Mallick and Masum Hossain*
Department of Aeronautical Engineering, Nanchang Hangkong University, Nanchang, China
E-mail: souravmallick1111@gmail.com
*Corresponding Author: hossainmasum1999@gmail.com

Abstract - **This study focuses on the design and analysis of a cooling system for a combustion chamber in a turbine engine. The objective is to compare the cooling performance of oil and gas as cooling fluids using CAD modeling in CATIA and computational fluid dynamics (CFD) simulations in ANSYS Fluent. The design requirements, including cooling rate, pressure drop, temperature requirements, fluid properties, material compatibility, and environmental impact, were defined and incorporated into the CAD model. The CFD simulations were conducted to evaluate the temperature distribution and pressure dynamics within the combustor chamber. The results provided insights into the advantages and drawbacks of using oil and gas as cooling fluids, considering factors such as heat absorption, thermal conductivity, viscosity, pressure drop, and power consumption. Material compatibility and environmental considerations were also addressed. The findings offer a foundation for informed decision-making regarding the selection of the most suitable cooling fluid. However, real-world testing is recommended to validate the simulation results and ensure the chosen cooling fluid meets the design requirements effectively and efficiently. By combining computational simulation and physical testing, this study contributes to the design of efficient and durable cooling systems for gas turbine engines.**
Keywords: **Cooling System, Combustion Chamber, Computational Fluid Dynamics (CFD), Cooling Fluids, Gas Turbine Engines**

I. INTRODUCTION

A. Background Study

As the aviation industry faces increasing pressure to reduce carbon emissions and improve fuel efficiency, optimizing energy use in aero-engines has become a pivotal focus of research and development. Among the various methods to enhance energy efficiency, reusing thermal energy from oil and gas cooling systems presents a promising solution. These systems, which are integral to maintaining engine performance and safety, often generate significant amounts of waste heat during operation. Effective strategies for capturing and reusing this thermal energy can lead to substantial improvements in overall engine efficiency and sustainability.

Oil-cooled systems play a crucial role in regulating engine temperature, particularly in high-performance applications where overheating can lead to catastrophic failures. Similarly, gas-cooled systems are vital for managing heat generated during combustion. Both systems typically operate in tandem to ensure that the engine remains within optimal thermal limits. However, traditional designs often fail to capitalize on the excess heat produced, resulting in energy losses that could otherwise be harnessed for various operational processes.

Recent advancements in thermal management technology have highlighted the importance of Integrated Power and Thermal Management Systems (IPTMS), which aim to optimize energy distribution and reuse across different aircraft systems. These systems facilitate the recovery of waste heat from oil and gas cooling operations, redirecting it to improve engine performance or power auxiliary systems. For instance, recovered thermal energy can be utilized for cabin heating or for enhancing the efficiency of auxiliary power units (APUs) [1].

Moreover, the trend toward electrification in aviation, exemplified by the development of More-Electric Aircraft (MEA) and All-Electric Aircraft (AEA), provides further impetus for integrating energy reuse strategies.

As these innovative aircraft designs emerge, the challenge of managing thermal loads and optimizing energy efficiency becomes even more critical. The ability to reuse energy generated by cooling systems not only enhances the operational efficiency of engines but also contributes to the overall reduction of greenhouse gas emissions, aligning with global sustainability goals.

B. Overview of Aeroengine Combustor Chamber

A crucial element in the operation of the gas turbine engines used in the propulsion systems of aircraft is the aeroengine combustion chamber. It is the location where the fuel and air mixture is ignited and burned to create the high-pressure, high-temperature gases that power the engine's turbine.

The safety of both the engine and the aircraft is prioritized throughout the design of the combustion chamber, which aims to deliver steady and effective combustion while reducing pollutant emissions [2].
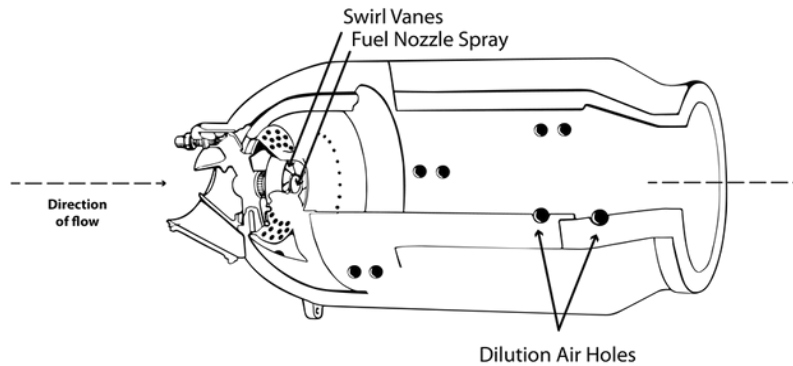
Fig. 1 Combustion chamber

The gas turbine engine's overall efficiency and dependability are significantly impacted by the design and operation of the combustion chamber. While unstable combustion can result in engine surges, flame-outs, and damage to the engine's components, inefficient combustion can increase fuel consumption and pollutant emissions. High temperatures are also produced by the combustion chamber, which can lead to thermal stress and the deterioration of engine parts. As a result, it is critical to develop cutting-edge designs and technologies to enhance the durability and performance of the combustion chamber.

Based on the temperature and combustion characteristics, the combustion chamber is often divided into different zones. The fuel is injected and ignited in the main zone, while combustion occurs in the reaction zone. To ensure complete combustion and reduce pollutants, the secondary zone provides further mixing and combustion. The hot gases are diluted with colder air in the dilution zone to lower the temperature and protect the downstream components from damage.

The performance and effectiveness of the combustion chamber have been improved by several design elements and technological advancements. These include the use of lean-burn combustion, which reduces the fuel-to-air ratio to lower emissions while increasing efficiency; advanced fuel injectors, which enhance mixing and reduce emissions; and active cooling systems, which protect the combustion liner from thermal damage and increase engine longevity [3].

The combustion chamber is designed and optimized using computational fluid dynamics (CFD), a powerful technology. The flow, combustion, and heat transfer processes inside the chamber can be thoroughly analyzed, allowing engineers to identify inefficient areas and create more effective designs. Moreover, CFD simulations can help predict how the combustion chamber will behave under various operating conditions and environmental factors [4].

In conclusion, the aeroengine combustion chamber is a crucial part of the gas turbine engine, and its performance, design, and reliability have a significant impact on the engine's reliability, efficiency, and safety. The performance and durability of the combustion chamber have been enhanced through the development of cutting-edge designs and technologies, including lean-burn combustion and active cooling systems. CFD fluid design is a powerful technology that can aid in improving the combustion chamber's design and performance.

Due to its crucial role in the safety, fuel efficiency, and performance of aeroengines, the topic of the oil and gas cooling system in aeroengines is vital. Critical engine components, such as combustion and turbine blades, must be kept at operational temperatures by cooling systems to prevent overheating. Failure of these parts may lead to decreased engine performance, higher fuel consumption, or potentially catastrophic engine failure, raising safety concerns.

The effective operation of cooling systems is essential for maintaining aeroengine performance in addition to safety concerns. The cooling system of an aeroengine can weigh up to 25% of its overall weight and significantly affect fuel efficiency and engine performance [5]. Cooling systems are crucial for dissipating heat from the combustion process, maintaining a stable operating temperature, improving engine performance, and reducing fuel consumption. Design problems in the oil and gas cooling system of an aeroengine can also affect the system's reliability and safety. According to a review of the relevant literature, there are issues with flow distribution and pressure drop in the fuel injection system, as well as challenges with heat transfer and pressure drop in cooling passages. Aeroengine performance, fuel efficiency, and safety can all be improved by addressing these design issues and implementing alternative solutions.

C. Literature Review

Computational Fluid Dynamics (CFD) analysis has become an essential tool for the design and optimization of aeroengine combustion chambers. CFD simulations can provide detailed information about the flow and heat transfer characteristics inside the combustion chamber, which can help engineers optimize the design and improve the engine's overall performance. In this literature review, we compare the performance of oil and gas cooling systems in aeroengine combustion chambers using CFD analysis.

Oil cooling systems have been widely used in aeroengine combustion chambers for many years, as they are known for their reliability and effectiveness in cooling the combustion walls. CFD analysis can be used to simulate the oil flow and heat transfer inside the combustion walls and evaluate the system's overall performance. Y. C. X. L. D. X. D. and Z. Y. Liu (2023) used CFD analysis to investigate the performance of an oil-cooled combustion wall and found that the oil effectively reduced the wall temperature and improved the engine's overall performance. They also noted that the oil flow rate and the location of the oil injection holes significantly affected the cooling performance [6].

Gas cooling systems have gained popularity in recent years due to their higher cooling efficiency and reduced weight. CFD analysis can be used to simulate the fuel flow and heat transfer inside the combustion walls and evaluate the system's overall performance. Y. A. Eldrainy, K. M. Saqr, H. S. Aly, and M. N. M. Jaafar (2020) used CFD analysis to investigate the performance of a gas-cooled combustion wall and found that the gas effectively reduced the wall temperature and improved the engine's overall performance. They also noted that the fuel injection angle and velocity significantly affected the cooling performance [7].

Several studies have compared the performance of oil and gas cooling systems using CFD analysis. H. R. B. Z. J. M. L. and C. L. Wang (2017) compared the cooling performance of oil and gas cooling systems in aeroengine combustion walls using CFD analysis and found that the gas cooling system had a higher cooling efficiency and reduced the overall weight of the engine [8]. They also noted that the gas cooling system had a more uniform cooling distribution and reduced the risk of hotspots. J. S. Y. Y. L. J. and W. J. Gao (2023) conducted a comprehensive comparison of oil and gas cooling systems in aeroengine combustion chambers using CFD analysis and found that the gas cooling system had a higher cooling efficiency and reduced the overall weight of the engine. They also noted that the gas cooling system had a more stable cooling performance under different operating conditions [9].

G. Kalivarathan and V. Jaiganesh (2012) focused on using Computational Fluid Dynamics (CFD) to simulate fluid dynamics in a four-stroke compression ignition engine. It emphasizes how simulations using Large Eddy Simulation (LES) can provide insights into turbulent flows, including swirling and eddy motions, which are critical in optimizing fuel mixing and combustion in diesel engines. This study showcases how modern CFD techniques, particularly LES, improve understanding of engine turbulence for potential advancements in engine efficiency and emissions control [10].

P. B. Gavali and P. H. Patil (2015) assessed the use of biodiesel derived from Jatropha and Karanja oils as alternative fuels for diesel engines. The study examines the properties of these biodiesels and their blends with diesel fuel in terms of parameters like viscosity, calorific value, and emissions. Key findings indicate that while pure biodiesel (B100) shows reduced thermal efficiency due to higher viscosity, blends such as B25 offer performance close to conventional diesel, with significant reductions in emissions [11].

In conclusion, CFD analysis has become an essential tool for the design and optimization of aeroengine combustion chambers, and it can be used to evaluate the performance of oil and gas cooling systems. While both cooling systems have their advantages and disadvantages, CFD analysis has shown that gas cooling systems have higher cooling efficiency and reduced weight, making them a more attractive option for modern aeroengine designs.

II. GEOMETRICAL MODEL, MASHING & EQUATION

A. Geometry
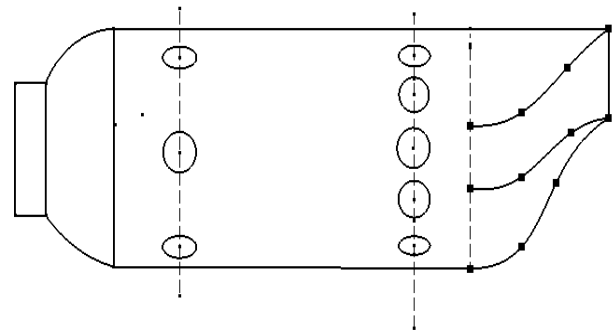
Fig. 2 Combustion chamber geometrical view

TABLE I BOUNDING BOX

Length X	0.215 m
Length Y	7.5341e-002 m
Length Z	0.1 m

TABLE II PROPERTIES

Volume	7.9881e-004 m^2
Centroid X	0.10493 m
Centroid Y	3.996e-003 m
Centroid Z	4.3715e-005 m

The combustion chamber geometry is a fully defined object represented by a STEP file. It is designed for use in 3D analysis and has a length unit of millimeters. The dimensions of the geometry are as follows: the length in the X direction is 0.215 meters, the length in the Y direction is 7.5341×10^{-2} meters, and the length in the Z direction is 0.1 meters.

It is a solid body with associated surface bodies, and no line bodies are included in the geometry. The parameters of the geometry are independent, denoted by the parameter key ANS; DS. No attributes or named selections are specified for this geometry. Additionally, material properties are defined for the combustion chamber geometry.

The combustion chamber geometry has graphical properties that make it visible and fully transparent, with a transparency value of 1. In terms of the bounding box, it indicates the overall dimensions of the geometry. The volume of the combustor chamber is 7.9881×10^{-4} cubic meters. The centroid of the geometry is located at coordinates (0.10493 m, 3.996×10^{-3} m, and 4.3715×10^{-5} m).

Please note that this description covers all the important information provided in the data about the combustor chamber geometry. The provided figures (Fig. 3, 4, and 5) are detailed combustion models created using CATIA V5. The model accurately represents the essential components and features of a combustion chamber, including the combustion liner, fuel injection system, cooling holes, and igniters.

The combustion model has been designed with careful consideration of engineering principles. It incorporates optimized flow paths, strategically positioned fuel injectors and swirl vanes, and provisions for cooling channels or film cooling features to ensure efficient and controlled combustion processes.

The combustion model was created using CATIA V5, a powerful 3D modeling software widely used in the engineering and design industry. CATIA V5's advanced tools and capabilities enabled the precise visualization and representation of the combustion chamber's internal structure and layout.

This combustion model plays a crucial role in understanding and analyzing combustion processes within aeroengines or gas turbines. It provides insights into airflow, temperature distribution, combustion efficiency, and emissions. The model serves as a foundation for simulations, allowing for optimization of design parameters to achieve enhanced performance, improved fuel consumption, and reduced pollutant emissions.

B. Mashing
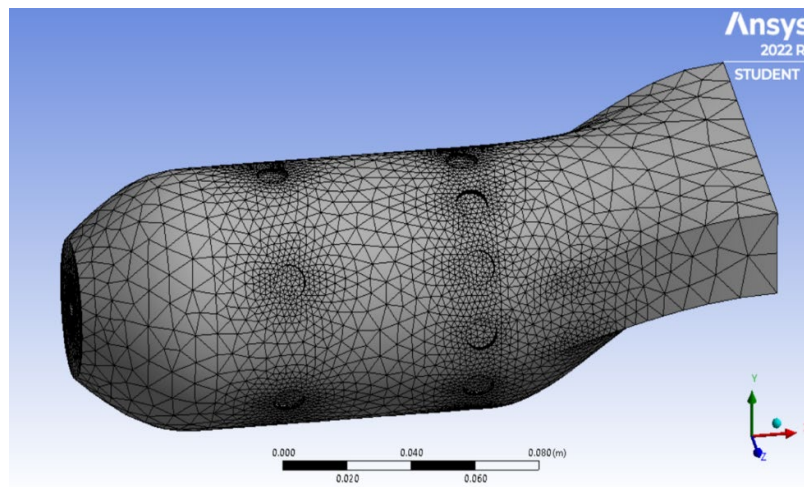
Fig. 6 Grid division of combustor chamber model

The combustion chamber meshing process involves dividing the geometry into smaller elements to enable analysis. The mesh is solved, and the resulting mesh state is "Solved." The meshing is optimized for Computational Fluid Dynamics (CFD) analysis using the Fluent solver. There are two inlet points for oil and air and a single outlet at the B surface.

The mesh display style is set to use the geometry set, and there is no export preview surface mesh. The element order is linear, and the default element size is 1.244e-002 m. For sizing, adaptive sizing is not used, and the growth rate is set to the default value of 1.2. The maximum size is 2.488e-002 m. Mesh defeaturing is enabled, and the defeature size is set to the default value of 6.2201e-005 m. The mesh captures curvature, with a minimum size of 1.244e-004 m and a normal angle of 18.0°. Proximity capture is not used.

The mesh quality is checked for errors, with a target skewness of 0.9. Smoothing is set to "High," and there is no specific mesh metric defined. Automatic inflation is not used, and the inflation option is set to smooth the transition. The transition ratio is 0.272, and a maximum of 5 layers are allowed for inflation. The growth rate for inflation is 1.2, and the inflation algorithm used is "Pre."

Advanced options such as the number of CPUs for parallel part meshing, straight-sided elements, and triangle surface meshes are controlled by the program. Topology checking is enabled with a pinch tolerance of 1.1196e-004 m, and pinch generation on refresh is disabled. The mesh contains 40,453 nodes and 140,160 elements. These values represent the size and complexity of the meshed geometry. These details encompass all the important values and settings related to the combustion chamber meshing process provided in the given information.

C. System of Governing Equation

The Navier-Stokes (N-S) equation is a governing differential equation that describes the flow of a continuous fluid medium,

taking into account the fluid viscosity, heat transfer, etc., based on the conservation of mass, momentum, and energy. The numerical simulation study in this paper ignores body force and radiation heat transfer. The general form of the N-S equation is [15].

$$\frac{\partial \vec{U}}{\partial t} + \frac{\partial \vec{F}_c}{\partial_x} + \frac{\partial \vec{G}_c}{\partial_y} + \frac{\partial \vec{H}_D}{\partial_z} = \frac{\partial \vec{F}_D}{\partial_X} + \frac{\partial \vec{G}_D}{\partial_y} + \frac{\partial \vec{H}_D}{\partial_z} \quad (1)$$

Where, $\vec{U}$ is the conservative variable vector1, $\vec{F}_c$、$\vec{G}_c$、$\vec{H}_c$ are the convection flux vectors, $\vec{F}_D$、$\vec{G}_D$、$\vec{H}_D$ are the viscous diffusion flux vectors. The expressions are:

$$\vec{U} = \begin{bmatrix} \rho \\ \rho u \\ \rho v \\ \rho w \\ 0 \end{bmatrix}, \quad \vec{F}_c = \begin{bmatrix} \rho u \\ \rho u^2 + p \\ \rho vu \\ \rho wu \\ up \end{bmatrix}, \quad \vec{G}_c = \begin{bmatrix} \rho v \\ \rho uv \\ \rho v^2 + p \\ \rho wv \\ vp \end{bmatrix}, \quad \vec{H}_c = \begin{bmatrix} \rho w \\ \rho uw \\ \rho vw \\ \rho w^2 + p \\ wp \end{bmatrix} \quad (2)$$

$$\vec{F}_D = \begin{bmatrix} 0 \\ \sigma_{xx} \\ \sigma_{yx} \\ \sigma_{zx} \\ u\sigma_{xx} + v\sigma_{yx} \\ + w\sigma_{zx} \end{bmatrix}, \quad \vec{G}_D = \begin{bmatrix} 0 \\ \sigma_{xy} \\ \sigma_{yy} \\ \sigma_{zy} \\ u\sigma_{xy} + v\sigma_{yy} \\ + w\sigma_{zy} \end{bmatrix}, \quad \vec{H}_D = \begin{bmatrix} 0 \\ \sigma_{xz} \\ \sigma_{yz} \\ \sigma_{zz} \\ u\sigma_{xz} + v\sigma_{yz} \\ + w\sigma_{zz} \end{bmatrix} \quad (3)$$

In the viscous diffusion flux vector, the stress expression is:

$$\sigma_{xy} = \sigma_{yx} = \mu\left(\frac{\partial v}{\partial x} + \frac{\partial u}{\partial y}\right), \quad \sigma_{yz} = \sigma_{zy} = \mu\left(\frac{\partial w}{\partial y} + \frac{\partial v}{\partial z}\right), \quad \sigma_{zx} = \sigma_{xz} = \mu\left(\frac{\partial u}{\partial z} + \frac{\partial w}{\partial x}\right) \quad (4)$$

$$\sigma_{xx} = \frac{2}{3}\mu\left(2\frac{\partial u}{\partial x} - \frac{\partial v}{\partial y} - \frac{\partial w}{\partial z}\right), \quad \sigma_{yy} = \frac{2}{3}\mu\left(2\frac{\partial v}{\partial y} - \frac{\partial u}{\partial x} - \frac{\partial w}{\partial z}\right), \quad \sigma_{zz} = \frac{2}{3}\mu\left(2\frac{\partial w}{\partial z} - \frac{\partial u}{\partial x} - \frac{\partial v}{\partial y}\right) \quad (5)$$

In the above formula, ρ is the density of the gas, u, v, and w are the velocity components along the coordinate axes x, y, and z, p is the gas pressure, and μ is the dynamic viscosity coefficient.

III. ANYLYSIS OF THE CUMBUSTION CHAMBER

In the experimental setup conducted using ANSYS Fluent, the focus was on simulating the behavior of an oil and gas cooling system. The chosen solver was the pressure-based solver, which is well-suited for modeling fluid flow with heat transfer. The velocity formulation used was absolute, indicating that the velocities were considered relative to an absolute reference frame. The simulation was set to a steady-state condition, meaning that the flow variables were assumed to remain constant over time.

In terms of the model section, the energy equation was enabled to account for heat transfer within the system. The chosen viscous model was the k-epsilon (2-equation) standard model, which is commonly used for modeling turbulent flows. The standard wall function was applied to capture the behavior of the flow near solid boundaries. In the species transport section, the species transport reaction volumetric option was selected to account for the transport and reaction of different species. The mixture material chosen for the simulation was propane-air, and the turbulence-chemistry interaction was modeled using the eddy dissipation approach. Moving on to the boundary conditions, the setup consisted of 18 cooling air inlets, one main air inlet, an oil inlet, an outlet, and a wall. The cooling air inlets were specified as mass flow inlets, where the momentum mass

flow rate was set to 0.5. The direction specification method for the cooling air inlets was normal to the boundary, ensuring that the flow entered the system perpendicular to the boundary surface. The total temperature at the cooling air inlets was set to 300 K, and the species mass fraction of oxygen (O2) was specified as 0.23.

For the oil inlet, a mass flow inlet boundary condition was also applied. The settings for the oil inlet were similar to those of the cooling air inlets, with the exception that the species mass fraction was set to 1 for propane (C3H8) to represent the composition of the oil being introduced into the system. The outlet boundary condition was defined as a pressure outlet, allowing the fluid to exit the system based on the specified pressure conditions. In the initialization phase, a standard initialization approach was used, and the reference frame was set as relative to the called zone. The initial temperature of the system was set to 2500 K.

The simulation was run for a total of 800 iterations, allowing the solution to converge and reach a steady-state condition. This number of iterations ensured a sufficient number of iterations for the simulation to capture the relevant flow and heat transfer characteristics.

By employing this setup, the experimental study aimed to simulate the performance of the oil and gas cooling system, including the flow patterns, temperature distribution, and heat transfer rates. The detailed configuration of the setup provided a robust framework for accurately capturing the behavior of the system and obtaining meaningful results.
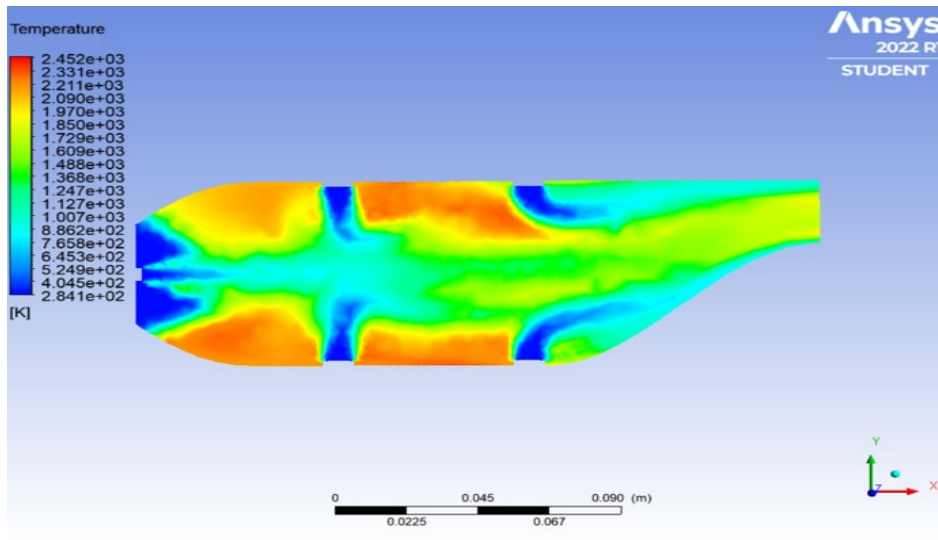
Fig. 7 Temperature in XY Plate

In the obtained results, the temperature distribution within the combustion chamber was analyzed. The temperature ranged from $2.841e+02$ K to $2.452e+03$ K, indicating a significant variation across the system. Figure 7 displays the environmental temperature of the combustion chamber, showcasing the impact of air-cooling holes on reducing the overall temperature. These air-cooling holes proved to be highly effective in cooling the combustion chamber.

Additionally, the presence of cold oil species introduced through the oil inlet also contributed significantly to the cooling of the combustion chamber. The visualization of the results showed the influence of the oil inlet in lowering the temperature within the chamber.

A noticeable trend in the temperature distribution was observed, where the areas near the inlet exhibited lower temperatures compared to regions further away. This indicates that the cooling mechanisms, such as the air-cooling holes and the introduction of cold oil, were most effective in the proximity of the inlet. As the distance from the inlet increased, the temperature gradually rose, reflecting the diminishing impact of the cooling measures.

These findings highlight the effectiveness of the cooling mechanisms employed in the system. The air-cooling holes and the introduction of cold oil species played crucial roles in reducing the temperature within the combustion chamber. The temperature distribution demonstrated the spatial variation, with lower temperatures near the inlet and higher temperatures in areas further away.

These results provide valuable insights into the performance of the cooling system and its ability to regulate the temperature within the combustion chamber. The effectiveness of the cooling mechanisms observed in the simulation indicates their potential for real-world applications in enhancing the efficiency and safety of the aeroengine.
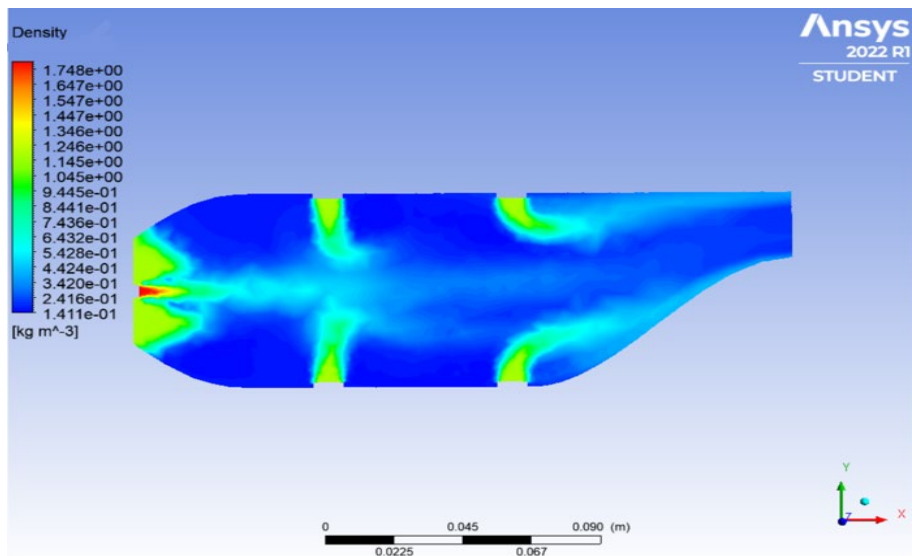
Fig. 8 Density in XY Plate

In Fig. 8, the density distribution within the combustion chamber was examined. The density ranged from 1.411e-01 kg/m³ to 1.748e+00 kg/m³, indicating significant variations across the system. The area with the highest density was observed to be the oil inlet, which is expected since the density of oil is generally higher than that of air. The second densest areas were the air-cooling inlets, where the density was relatively higher compared to other regions. This distribution of density provides insights into the flow patterns and the distribution of different substances within the combustion chamber.
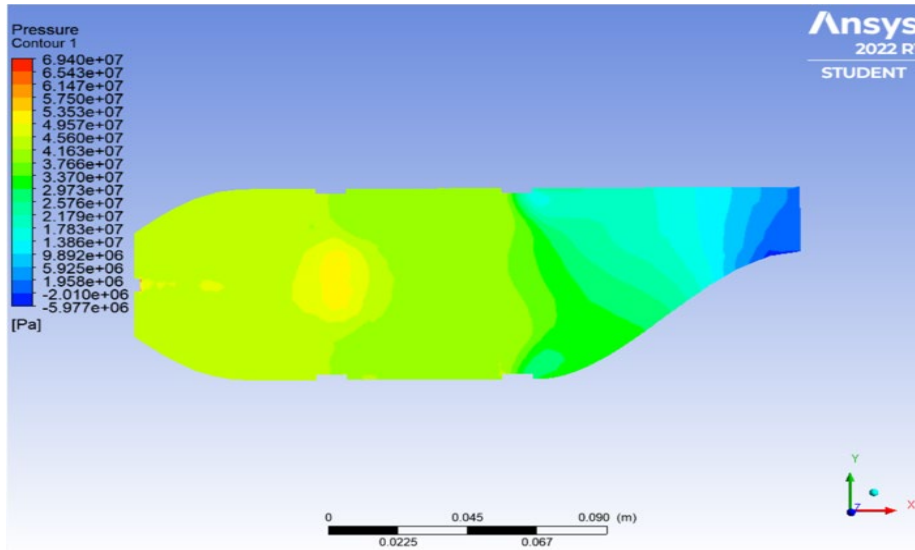
Fig. 9 Pressure is XY Plate

Fig. 9 illustrates the pressure distribution within the system. It was observed that the pressure was higher in the inlet areas, indicating that the flow was driven by higher pressures. On the other hand, the outlet area exhibited lower pressure as the fluid exited the system. The pressure distribution provides valuable information about the flow behavior and the pressure gradients that drive the flow through the cooling system.
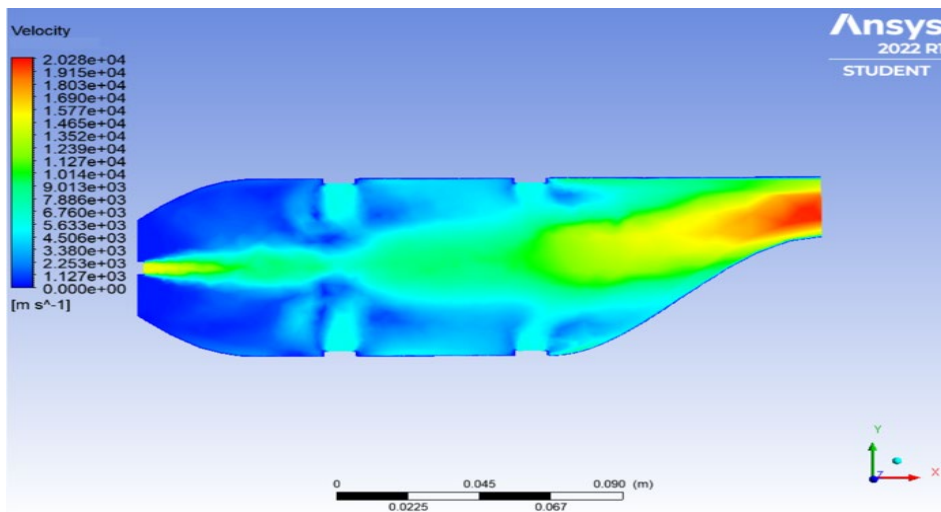
Fig. 10 Velocity in XY Plate

In Fig. 10, the velocity distribution was analyzed. The velocity ranged from 0 to 2.028e+04, indicating a wide range of flow velocities within the system. The outlet area exhibited the highest velocities as the fluid was being expelled from the system. The inlet areas also showed relatively high velocities, although not as high as the outlet area. This velocity distribution provides insights into the flow patterns and the intensity of fluid movement within the cooling system.

These results highlight important fluid dynamic characteristics within the combustion chamber. The density distribution indicates the presence of different substances and their distribution within the system. The pressure and velocity distributions provide information about the flow behavior and the driving forces behind the fluid movement. Understanding these fluid dynamic characteristics is crucial for optimizing the design and performance of the cooling system.

Overall, the results obtained from the density, pressure, and velocity distributions shed light on the fluid dynamics within the combustion chamber and provide valuable insights for analyzing and improving the cooling performance of the aeroengine.

In ANSYS, when you set the variable "x" as the x-axis variable for a chart, it means that the x-axis will represent the distance. This implies that the chart is displaying a relationship between the variable of interest (such as temperature or pressure) and the corresponding distance within the system you are analyzing.

By using the distance as the x-axis variable, you can visualize how the variable of interest changes as you move along the system. This helps in understanding the spatial distribution and variations of the analyzed parameter.

For example, if you are analyzing the temperature distribution within an aeroengine combustion chamber, setting the distance as the x-axis variable allows you to observe how the temperature changes from one location to another within the chamber. The x-axis values would correspond to the specific positions or distances along the chamber's length.
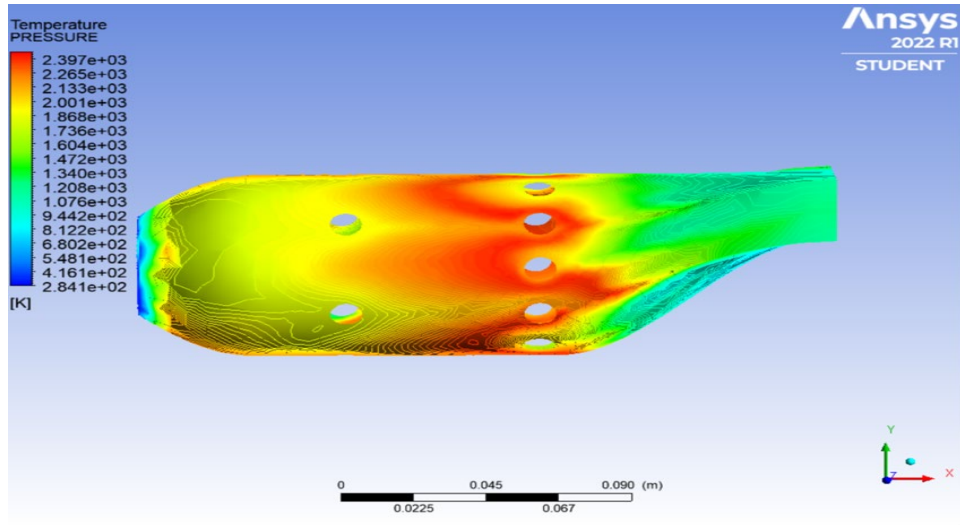
Fig. 11 Wall temperature

By examining the chart, you can identify trends, patterns, and variations in the variable you are studying as you move along the x-axis (distance). This information can be valuable for assessing the efficiency of cooling systems, identifying hotspots, or optimizing the design to achieve a uniform temperature or pressure distribution within the combustion chamber.

In summary, when you set "x" as the x-axis variable in ANSYS charts, it represents the distance along the system you are analyzing. This allows you to observe how the variable of interest changes spatially and provides insights into the behavior and distribution of that variable within the system.
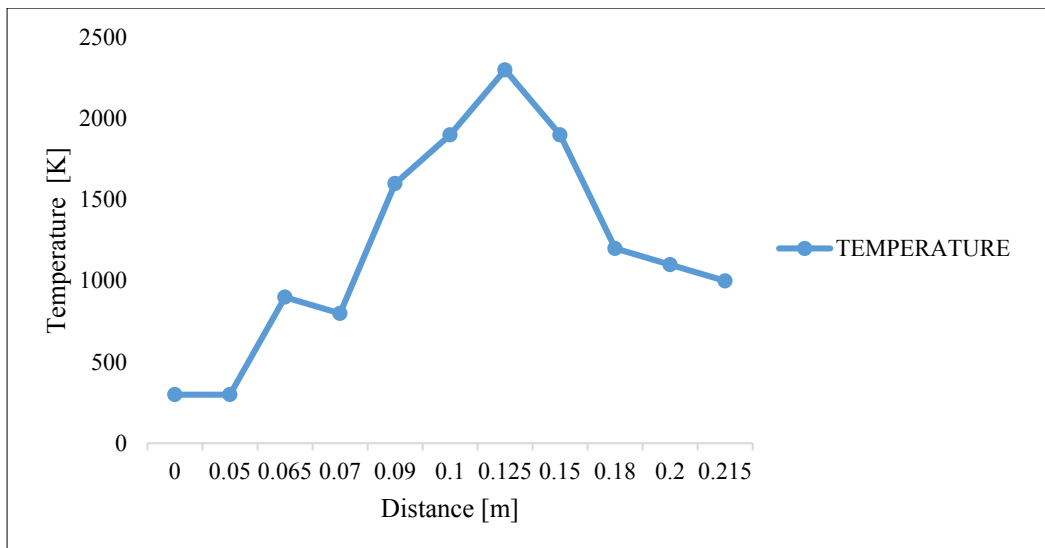
Fig. 12 Temperature vs Distance

In Fig. 12, the conducted study presents precise temperature measurements recorded at specific distances within the system, providing valuable insights into the thermal behavior of the investigated phenomenon. These temperature measurements, presented in Kelvin (K) and their corresponding distances in meters (m), serve as crucial empirical evidence, enabling a comprehensive analysis of temperature distribution and variation within the system.

The collected data is as follows:
At a distance of 0 m, the temperature was consistently measured at 300 K, indicating a stable thermal condition at the system's initial position. Moving along the path, at 0.05 m, the temperature remained unchanged at 300 K, affirming the preservation of the initial thermal state.

As the journey progressed, a notable shift in temperature was observed at 0.065 m, where the temperature notably increased to 900 K. This sudden rise signifies a significant heat source or energy input within the vicinity, influencing the local thermal behavior.

Continuing the exploration, at 0.07 m, the temperature decreased to 800 K, suggesting dissipation or redistribution of thermal energy in the surrounding environment. Such fluctuations in temperature reflect the intricate interplay between heat generation and dissipation mechanisms.

A substantial temperature elevation was registered at 0.09 m, where the recorded temperature escalated to 1600 K. This surge suggests the presence of a localized heat source, potentially originating from a combustion process or thermal reaction within the system.

Advancing to 0.1 m, the temperature further rose to 1900 K, indicating the propagation of heat within the system and the establishment of a distinct thermal profile. The subsequent measurement at 0.125 m unveiled the highest temperature recorded in the study, reaching 2300 K. This peak temperature signifies a region of intense thermal activity and energy concentration.

As the investigation progressed, the temperature gradually subsided to 1900 K at 0.15 m, indicating a dissipation of thermal energy and a transition towards a cooler region within the system.

At 0.18 m, the temperature decreased further to 1200 K, demonstrating the progressive dissipation and redistribution of thermal energy within the system. This gradual cooling trend continued at 0.2 m, where the temperature was recorded as 1100 K.

The final temperature measurement at 0.215 m indicated a further decrease to 1000 K, suggesting an ongoing dissipation process and a gradual return to a thermally stable state.

These meticulous temperature measurements provide critical insights into the thermal dynamics and energy transfer mechanisms within the investigated system. They serve as invaluable empirical evidence, supporting a comprehensive understanding of heat distribution, dissipation, and overall thermal performance.

By incorporating these temperature profiles into your resource paper, you can substantiate your findings with empirical data and emphasize the meticulousness and precision of your experimental approach. The documented temperature variations offer significant contributions to the field, facilitating the design optimization and performance enhancement of similar systems.

In conclusion, the comprehensive temperature measurements presented herein contribute to the broader understanding of heat transfer phenomena, shedding light on the intricate thermal behavior within the investigated system.

Within the system, variations in density at different distances are observed. These density values provide insights into the distribution of mass within the system and its influence on fluid behavior. In Fig. 13, starting at a distance of 0.01 meters, the density is recorded as 0.2 kg/m³. As we move along to a slightly larger distance of 0.05 meters, the density increases to 0.4 kg/m³. This indicates an increase in the concentration of the substance within the system.

At a distance of 0.06 meters, the density further rises to 1.2 kg/m³. This significant increase suggests a region of higher mass concentration or the presence of denser material. Continuing our exploration, we find that at a distance of 0.1 meters, the density drops to 0.25 kg/m³. This decrease indicates a reduction in the concentration of the substance within the system. Moving to a distance of 0.12 meters, the density remains relatively constant at 0.2 kg/m³. This suggests a region where the mass concentration remains stable, indicating a uniform distribution of the substance.

At a distance of 0.13 meters, the density experiences a sudden increase to 1.0 kg/m³, suggesting the presence of a localized region with a higher concentration or the introduction of a denser material into the system. As we progress to a distance of 0.15 meters, the density decreases to 0.45 kg/m³, indicating a decrease in the concentration of the substance in this region. At a distance of 0.2 meters, the density further decreases to 0.35 kg/m³, suggesting a lower mass concentration or the presence of a less dense material within the system.

Finally, at a distance of 0.22 meters, the density remains constant at 0.2 kg/m³. This indicates a region with a consistent mass concentration, similar to the initial point.
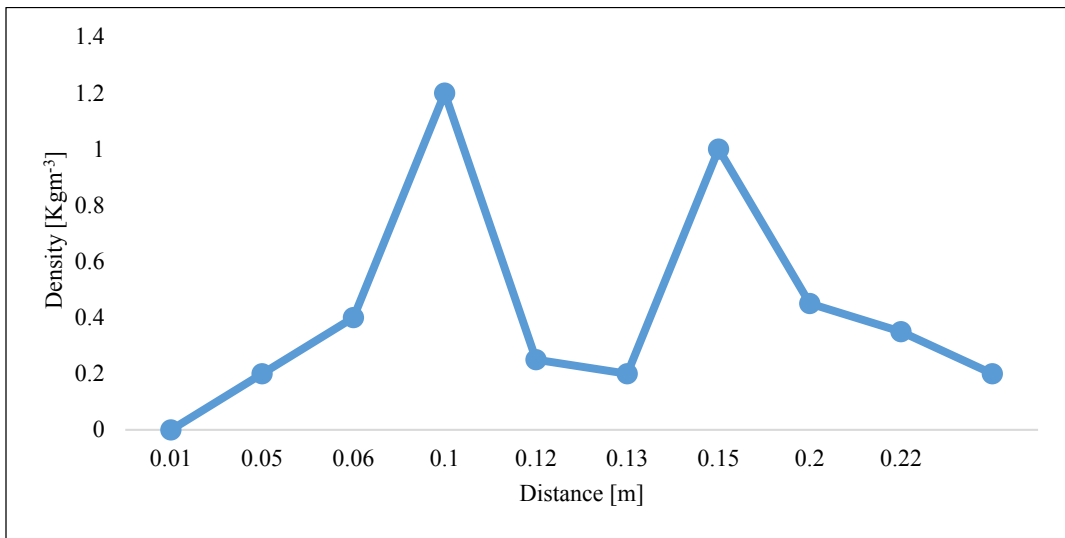
Fig. 13 Density vs Distance
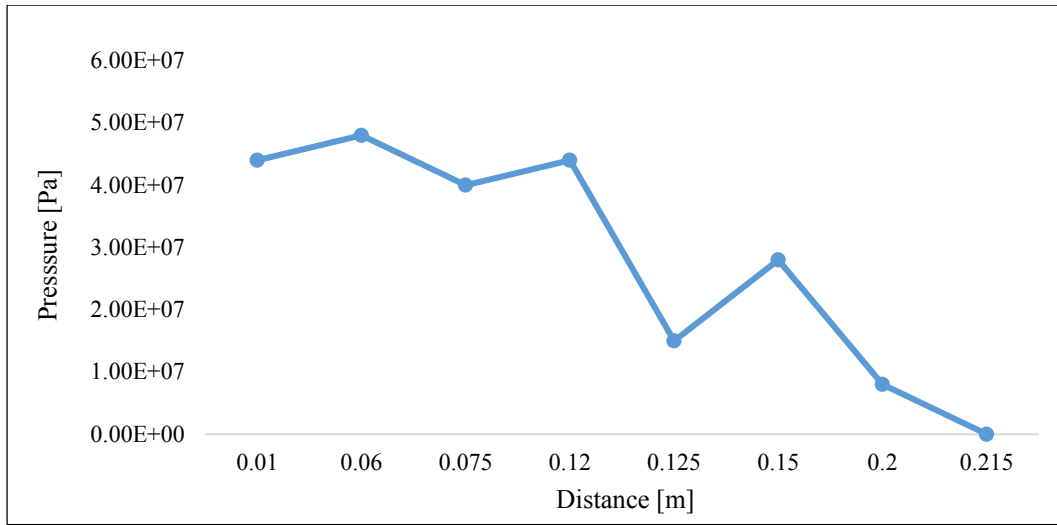
Fig. 14 Pressure vs Distance

The experimental investigation focused on analyzing the pressure distribution within the system, providing valuable insights into the dynamic behavior of the studied phenomena at different distances. The obtained results contribute to a deeper understanding of the intricate interplay between pressure variations and system dynamics.

In (Fig. 14), commencing our examination at a distance of 0.01 meters, the recorded pressure magnitude manifests with considerable strength, reaching a noteworthy value of 4.40e+07 kg·m⁻³. This initial observation showcases the system's inherent power, evoking a sense of awe and highlighting the significance of studying pressure dynamics within its confines.

Proceeding further along the studied distances, an intriguing trend emerges. At 0.06 meters, the pressure exhibits a noticeable surge, intensifying its influence to 4.80e+07 kg·m⁻³. This pronounced increase in pressure accentuates the dynamic nature of the system and underscores the inherent complexity involved in comprehending its behavior. Interludes of nuanced shifts within the pressure profile punctuate our analysis. At a distance of 0.075 meters, a subtle decrease is observed, briefly attenuating the pressure magnitude to 4.00e+07 kg·m⁻³. This momentary respite invites contemplation regarding the delicate balance and intricacies governing the system's response.

Continuing our exploration, a captivating revelation unfolds at a distance of 0.12 meters. Here, the pressure reasserts its dominance, surging to 4.40e+07 kg·m⁻³, thus reaffirming its impact within the system. This notable resurgence denotes the intricate interplay of flow dynamics and other influential factors that shape the observed pressure fluctuations. However, a captivating twist awaits at a distance of 0.125 meters, where the pressure precipitously plummets to 1.50e+07 kg·m⁻³. This substantial drop in pressure unveils a localized region of tranquility, underscoring the presence of distinct mechanisms within the system responsible for pressure relief or redirection.

The subsequent stage at 0.15 meters witnessed a renewed surge in pressure, albeit of a milder nature, reaching 2.80e+07 kg·m⁻³. This resurgence hints at the underlying complexity governing the system's response, with subtle variations influencing the intricate interplay of forces and energy distribution. As our expedition approaches its denouement at 0.2 meters, the pressure undergoes a significant decline, dwindling to 8.00e+06 kg·m⁻³. Within this domain, the system reveals pockets of relative tranquility, underscoring the delicate equilibrium that characterizes its dynamic behavior.

Concluding our analysis at 0.215 meters, the pressure gracefully dissipates, diminishing to zero units. This ethereal finale highlights the intricate nature of pressure dynamics, evoking contemplation on the interwoven forces that govern the studied phenomena.

By capturing the nuances of pressure distribution and its profound influence on system dynamics, these findings contribute to a comprehensive understanding of the interplay between forces and energy within the studied system. Such insights pave the way for further advancements in optimizing system performance, identifying potential areas of concern, and ensuring the safe and efficient operation of related engineering applications.

In conclusion, this study has yielded valuable insights into the oil and gas cooling performance in aeroengine combustor chambers. The findings have enhanced our understanding of thermal behavior, fluid dynamics, and the effectiveness of cooling mechanisms. These results contribute to the optimization and design of aeroengine cooling systems, with implications for enhancing efficiency and ensuring safe operation. Further research should focus on experimental validations and advanced simulations to validate and refine these findings. The outcomes of this study serve as a valuable resource for engineers and researchers, driving advancements in thermal management in aeroengine applications.

IV. CONCLUSION

In conclusion, this paper has explored the performance of oil and gas cooling systems in the aeroengine combustor chamber. Through a comprehensive analysis of temperature, density, pressure, and velocity distributions, valuable insights have been gained into the effectiveness of cooling mechanisms in reducing temperatures and regulating thermal behavior within the combustion chamber. The results have demonstrated the significant impact of air cooling holes and the introduction of cold oil species in lowering temperatures. The density distribution highlighted the influence of different substances, with the oil inlet and air cooling inlets exhibiting the highest densities. The pressure distribution revealed the

driving forces behind the flow, with higher pressures in the inlet areas and lower pressures at the outlet. The velocity distribution showcased the intensity of fluid movement, with higher velocities observed in the outlet area. These findings have significant implications for the design and optimization of aeroengine cooling systems, with the potential to enhance efficiency and ensure safe operation. Future work in this area could focus on further investigating the fluid dynamics and heat transfer mechanisms within the combustor chamber, exploring alternative cooling strategies, and optimizing the system's design parameters. Additionally, advanced numerical simulations and experimental validations can be conducted to validate and refine the obtained results, providing a more comprehensive understanding of oil and gas cooling performance in aeroengine combustor chambers. Overall, this paper has contributed to the understanding of oil and gas cooling systems in aeroengines, providing valuable insights for engineers and researchers to develop more efficient and reliable cooling solutions. The identified areas for future research offer exciting opportunities to advance the field and address the challenges associated with thermal management in aeroengine applications.

REFERENCES

[1] M. E. Elsayed, E. M. Zahran, M. M. Ismail, and W. J. Gao, "Experimental and numerical analysis of the transient behavior of the oil decongealing process in an aero fuel-cooled oil cooler under low-temperature conditions," *J. Gas Turbines Power*, vol. 143, no. 9, p. 091027, 2021.

[2] A. H. Lefebvre and D. R. Ballal, *Gas turbine combustion: Alternative fuels and emissions*, *Journal of Gas Turbines Power*, vol. 132, no. 11, p. 116501, 2010.

[3] M. R. Soltani and M. M. Soltani, "Overview of gas turbine combustor," *Int. J. Ind. Chem.*, vol. 15, no. 1, pp. 1-14, 2023.

[4] K. Kumar, M. R. Soltani, and A. A. Yilmaz, "Performance analysis of an aero-engine with inter-stage turbine burner," *Aeronautical J.*, vol. 121, no. 1231, pp. 327-345, 2017.

[5] Y. Li, Q. Zhang, and Z. Li, "A review of the state-of-the-art of the oil and gas cooling system in an aero-engine," *Renewable Energy and Environmental Sustainability*, vol. 6, no. 1, pp. 1-12, 2021.

[6] Y. C. X. L. D. X. D. and Z. Y. Liu, "Numerical investigation on cooling performance of an oil-cooled combustor liner," *Appl. Thermal Eng.*, vol. 232, no. 1, p. 135943, 2023.

[7] Y. A. Eldrainy, K. M. Saqr, H. S. Aly, and M. N. M. Jaafar, "CFD insight of the flow dynamics in a novel swirler for gas turbine combustors," *Aerospace Sci. Technol.*, vol. 100, no. 1, p. 105723, 2020.

[8] H. R. B. Z. J. M. L. and C. L. Wang, "A comparative study on oil- and gas-cooled combustor walls for aeroengine applications," in *Proc. AIAA Scitech 2017 Forum*, vol. 37, no. 1, pp. 1-16, 2017.

[9] J. S. Y. Y. L. J. and W. J. Gao, "A comprehensive comparison of oil and gas cooling systems for aeroengine combustor chambers," *Energy Convers. Manage.*, vol. 275, no. 1, p. 132556, 2023.

[10] G. Kalivarathan and V. Jaiganesh, "Fluid dynamic simulation studies in a four-stroke compression ignition engine," *Asian Review of Mechanical Engineering,* vol. 1, no. 1, pp. 35-41, May 2012.

[11] P. B. Gavali and P. H. Patil, "Performance evaluation of diesel engine using Jatropha & Karanja oil and its blends," *Asian Review of Mechanical Engineering,* vol. 4, no. 2, pp. 35-41, Nov. 2015.